


Article

Numerical Study on Performance Enhancement of the Air-Cooled Battery Thermal Management System by Adding Parallel Plates

Meiwei Wang ¹ , Tzu-Chen Hung ² and Huan Xi ^{1,*}

¹ Key Laboratory of Thermo-Fluid Science and Engineering of Ministry of Education, School of Energy and Power Engineering, Xi'an Jiaotong University, Xi'an 710049, China; zhoujy0813@stu.xjtu.edu.cn

² Department of Mechanical Engineering, National Taipei University of Technology, Taipei 10607, China; tchung@ntut.edu.tw

* Correspondence: huanxi@mail.xjtu.edu.cn

Abstract: Air-cooled battery thermal management system (BTMS) technology is commonly used to control the temperature distribution of the battery pack in an electric vehicle. In this study, parallel plates are introduced to improve the cooling efficiency of the BTMS, which can change the airflow distribution of the battery pack. Firstly, the effect of the number of parallel plates on the cooling performance of the BTMS is investigated; within the acceptable range of power consumption loss, the model with two parallel plates shows the best cooling efficiency, and T_{\max} and ΔT_{\max} are reduced by 2.42 and 3.46 K, respectively. Then, the influences of the length and height of parallel plates are studied; the optimal values for length and height are 1.5 and 30 mm, respectively. Finally, the conclusions drawn above are used to design three optimization schemes for the model with four parallel plates; the cooling efficiency of the battery pack can be improved efficiently, which illustrates the feasibility of the above conclusions. Compared to the original model, T_{\max} and ΔT_{\max} are, respectively, reduced by 3.37 K (6.17%) and 5.5 K (71.9%) after optimization.

Keywords: battery thermal management system; parallel plate; air-cooled; computational fluid dynamics; cooling performance



Citation: Wang, M.; Hung, T.-C.; Xi, H. Numerical Study on Performance Enhancement of the Air-Cooled Battery Thermal Management System by Adding Parallel Plates. *Energies* **2021**, *14*, 3096. <https://doi.org/10.3390/en14113096>

Academic Editor: Adrian Ilinca

Received: 3 April 2021

Accepted: 21 May 2021

Published: 26 May 2021

Publisher's Note: MDPI stays neutral with regard to jurisdictional claims in published maps and institutional affiliations.



Copyright: © 2021 by the authors. Licensee MDPI, Basel, Switzerland. This article is an open access article distributed under the terms and conditions of the Creative Commons Attribution (CC BY) license (<https://creativecommons.org/licenses/by/4.0/>).

1. Introduction

Today, the massive emission of carbon dioxide leads to the gradual aggravation of the greenhouse effect. To reduce the emission of carbon dioxide from the transportation industry, electric vehicles (EVs) are a good choice and have been developed rapidly in recent years [1]. The battery pack plays an important role in the component of an EV, and the economy, mileage, and power performance of EVs are determined by the performance of the battery packs [2]. Lithium-ion batteries are widely used in EVs due to the characteristic of high energy density and low self-discharge rate. The performance and life of lithium-ion batteries are closely related to temperature; the operating temperature of lithium-ion batteries should be controlled within the range of 25–40 °C [3], and the maximum temperature difference of the battery pack should be kept within 5 °C [4]. An extremely high temperature or temperature difference of the battery pack will accelerate the electrode degradation and the reduction in lithium-ion battery capacity, and even threats to the safety of EVs such as fire and explosion, while an extremely low temperature will increase the internal resistance and cause under-capacity of batteries [5].

To this end, it is necessary to design a rational and efficient battery thermal management system (BTMS) that can ensure the temperature and temperature difference of the battery pack within a normal range. The optimization of the cooling module and strategy has been widely studied. BTMS technology is mainly divided into three different types: air cooling, liquid cooling, and phase change material (PCM) cooling [6]. Compared to liquid

cooling technology and PCM cooling technology, air cooling technology has been employed extensively due to the advantages of low cost, long service life, and no additional weight.

The cooling performance can be enhanced by improving the flow pattern of the battery pack, and changing the structure of the model is an efficient choice. Peasaran et al. [7] compared the thermal performance for serial cooling and parallel cooling of a battery pack, and the results indicated that the one with parallel ventilation provided a lower maximum temperature of the battery pack and obtained better temperature uniformity. Based on the parallel air-cooled BTMS, the spacing among the cells and the cell arrangement were the focus of the research. Severino et al. [8] optimized the cell spacing by introducing computational intelligence techniques, and a trade-off between the area, temperature, and power consumption of the system was found; meanwhile, the maximum temperature and maximum temperature difference of the battery pack both obtained a decrease of 2 K. Chen et al. [9] proposed a novel optimization strategy of cell spacing among the battery cells; in the case of steady and unsteady heat generation rates, the maximum temperature difference of the battery pack was reduced by 29% and 37%, respectively. Wang et al. [10] compared the cooling performance in the same conditions under five battery arrangements, and the results showed that the best cooling capability and the lowest cost were achieved by the 5×5 cubic structure, but in terms of the space utilization and the cooling efficiency, axisymmetric module structure was a better choice. It is also an effective way to acquire a different flow pattern by adjusting the position of the inlet and outlet of the BTMS. Nine kinds of air-cooled systems with different inlet and outlet location were proposed by Chen et al. [11], and the flow and temperature fields were calculated and compared; it was found that when the inlet and outlet were both located at the middle of the module, the system obtained the best cooling performance. The influence of the quantity of the inlet and outlet has also been studied. Hong et al. [12] introduced a second outlet to the battery pack, and the influences of the position and size of the second vent on cooling efficiency were studied; the numerical calculation results showed that when the secondary vent was located against the outlet of the system, the maximum temperature of the battery pack was reduced by 5 K, and the maximum temperature difference was reduced by 60%. Shahid al. [13] added a secondary inlet to change the direction of the airflow, and the cooling performance of the battery pack was significantly enhanced. Park [14] combined the secondary vent with the tapped ducts to increase the cooling efficiency of the air-cooled BTMS. The cooling performance can be improved by introducing the tapered inlet and outlet manifolds in particular. Xie et al. [15] designed a three-factor orthogonal experiment; the air inlet and outlet angle were optimized, and the maximum temperature and maximum temperature difference of the battery pack were reduced by 12.82% and 29.72%, respectively. Chen et al. [16] proposed an optimization strategy to obtain the optimal angles of the plenums, and the cooling efficiency was improved without the total volume and power consumption of the system.

The method of adding one or more partitions to the cooling module has been proven to be feasible. Shahid al. [17] added a thin separating plate to the air-cooled BTMS; the airflow was separated from the inlet plenum and the battery cells, and the best temperature performance of the battery pack was acquired when the separating plate length was 121 mm. Na et al. [2] added a transverse partition to the battery pack module, and the cooling flow was divided into multilayer flow channel; as a result, the maximum average temperature difference of the system was reduced by 1.1 K. Zhang et al. [18] added spoilers in the battery pack module directly under the cooling channel, and compared with the original model, the maximum temperature and maximum temperature difference of the optimal model, respectively, obtained a 6.66% and 94.24% reduction.

Therefore, it is a main method to improve the cooling performance by changing the airflow distribution in the BTMS. Previous studies have paid more attention to designing the high-efficiency cooling structure of the battery pack. There are few studies on improving the airflow distribution by adding a parallel plate in the cooling channel. Zhang et al. [18] added spoilers to the Z-type BTMS, and the influences of the inclination angle and height

of spoilers on cooling performance were studied. However, their work was not targeted, resulting in inefficiency, and the situation of spoiler installation in the cooling channel was not fully considered. In this study, the typical Z-type air-cooled BTMS was employed as the research object. To reduce the airflow into the cooling channel where the airflow velocity is higher, the parallel plates were installed at the side of the battery cells (in the cooling channel). The airflow velocity in each cooling channel was adjusted to be more uniform, and the cooling performance of the system could also be improved. The numerical computation method was employed to simulate and analyze the flow and temperature fields of the BTMS. The influence of the number of parallel plates on the cooling performance of the battery pack was investigated firstly. Then, the impact trends of the position and length of parallel plates were also studied. Finally, the influence rules of those factors were verified by applying them to one case. The method proposed in this study is feasible for providing a reference to enhance the cooling efficiency of other air-cooled BTMSs.

2. Materials and Methods

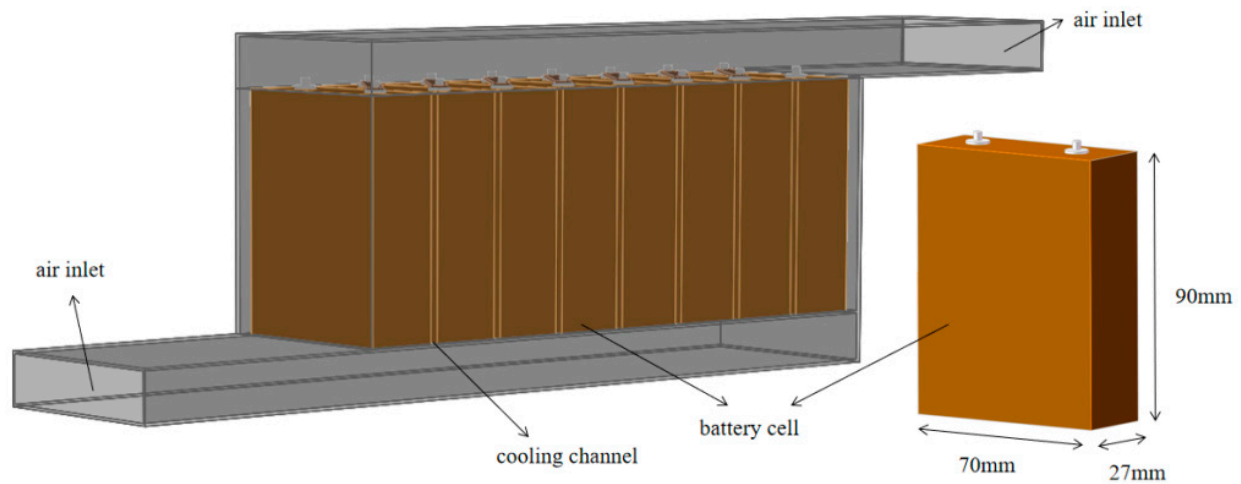
2.1. Physical Model

2.1.1. Battery Pack Model

In this paper, the Z-type air-cooled BTMS was employed, and the three-dimensional (3D) diagram of the model is shown in Figure 1a. In order to achieve efficient simulation, the positive and negative parts of the battery were ignored. Figure 1b shows the two-dimensional (2D) diagram of the battery pack. As shown in Figure 1, the Z-type air-cooled BTMS consists of eight prismatic battery cells (denoted as Bat1 to Bat8) and nine cooling channels (denoted as cooling channel1 to cooling channel9). The length, width, and height of the battery cell are $27 \times 70 \times 90$ mm. The height and length of the inlet and outlet manifolds are, respectively, set to 20 and 100 mm, and the width of each cooling channel is set to 3 mm. The specific details of the air and battery cell in Ref. [11] are summarized as follows: the specific heat, density, dynamic viscosity, and thermal conductivity of the air are $1005 \text{ J}/(\text{kg}\cdot\text{K})$, $1.165 \text{ kg}/\text{m}^3$, $1.86 \times 10^{-5} \text{ kg}/(\text{m}\cdot\text{s})$, and $0.0267 \text{ W}/(\text{m}\cdot\text{K})$, respectively, and the specific heat and density of the battery are $1337 \text{ J}/(\text{kg}\cdot\text{K})$ and $1542.9 \text{ kg}/\text{m}^3$, respectively. In this study, the 3D model was simplified into a 2D model, the properties and calculation in the direction of the length of the battery pack (70 mm) were ignored, and in the direction of height and width, the thermal conductivity of the battery was 1.05 and 21.1, respectively. The heat generation power of each battery cell was 11.8 W. The ambient temperature and inlet airflow velocity were set to 299.15 K and 3.5 m/s, respectively.

2.1.2. Parallel Plate Model

For the original air-cooled model, the airflow velocity in each cooling channel is not uniform, and the airflow velocities in the cooling channels near the air inlet are low, while those away from the air inlet are high, which leads to a large temperature difference of the battery pack. According to the above description, parallel plates were introduced to change the airflow distribution. The parallel plates were set to be adiabatic, and thickness was ignored. The number, length, and height of parallel plates can be adjusted, and the effects of these factors on the cooling performance of the battery pack are investigated in this paper. Figure 2 gives an example of the BTMS with two parallel plates.



(a)



(b)

Figure 1. Diagram of the Z-type air-cooled battery thermal management system (BTMS); (a) 3D diagram of the Z-type air-cooled battery thermal management system (BTMS); (b) 2D diagram of the Z-type air-cooled battery thermal management system (BTMS).

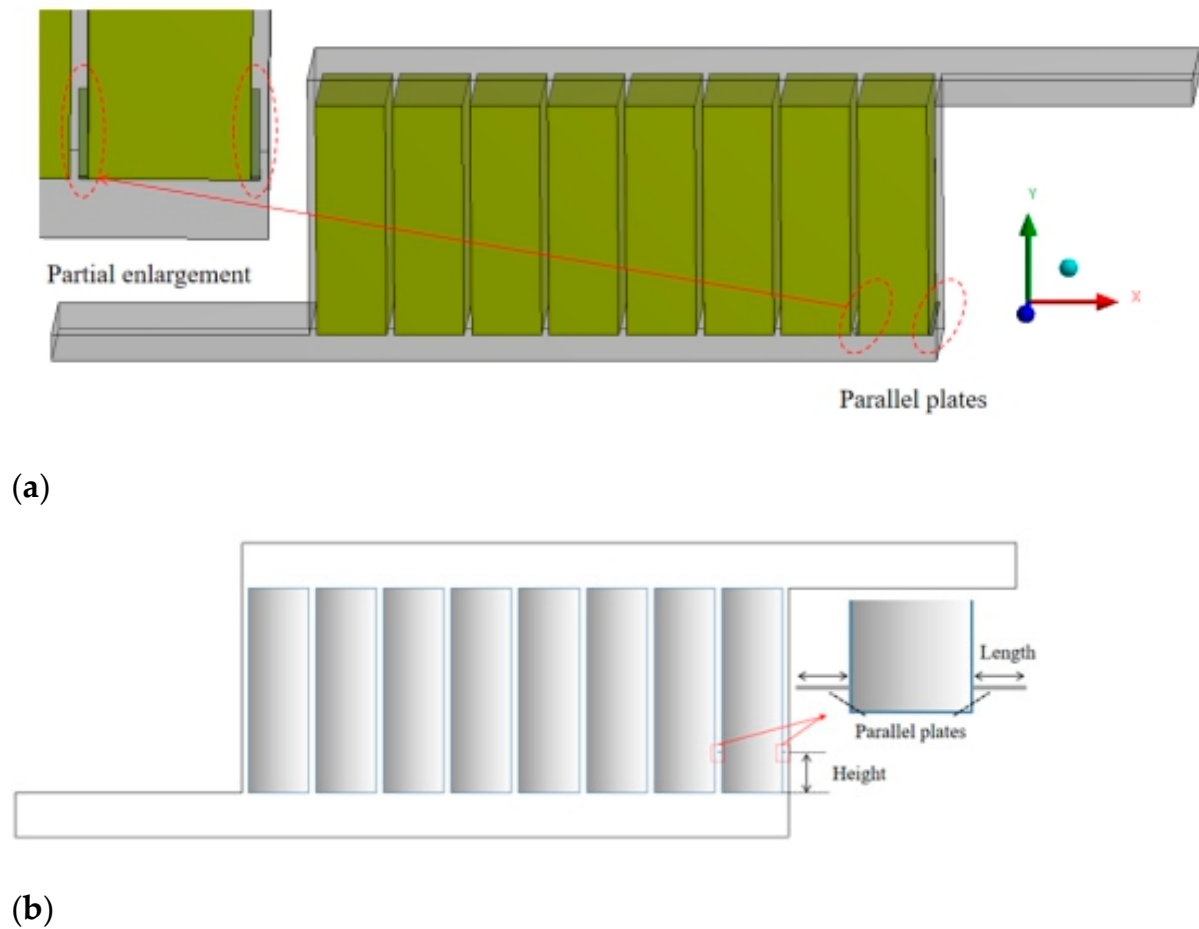


Figure 2. Battery thermal management system (BTMS) with two parallel plates; (a) 3D example of adding two parallel plates; (b) 2D example of adding two parallel plates.

2.2. Numerical Method

2.2.1. Numerical Model

In the present study, for an air-cooled BTMS, the maximum battery temperature (T_{\max}), the maximum temperature difference (ΔT_{\max}), and power consumption of the battery pack were chosen as the evaluation indexes of the cooling performance, where each battery temperature represents their average temperature. The computational fluid dynamics (CFD) method was employed to simulate the temperature and flow fields of the system. Power consumption is associated with the pressure drop (ΔP), and the equation to calculate the power consumption is:

$$W_P = (P_{in} - P_{out}) \times Q_0 \quad (1)$$

$$P = P_{in} - P_{out} \quad (2)$$

where W_P is the power consumption, Q_0 is the inlet air flow rate, and P_{in} and P_{out} are the average pressure at inlet and outlet sections. Due to the same inlet airflow velocity of all cases, ΔP was used to evaluate the capacity to consume power in this study. On account of the inlet airflow velocity of 3.5 m/s, which is much smaller than the acoustic velocity, air was treated as the incompressible fluid. Therefore, the Navier–Stokes (N-S) equation was chosen as the governing equation [19]. The Reynolds number was 6795 based on the inlet airflow velocity, which is larger than 3000, so the status of the airflow was regarded as turbulent flow. Therefore, the standard $k-\epsilon$ model was employed in this study, and the Enhanced Treatment was selected [18]. All the governing equations are shown below.

Continuity equation:

$$\nabla \cdot \vec{v} = 0 \quad (3)$$

Energy conservation equation:

$$\rho_a c_a \frac{\partial T_a}{\partial t} + \nabla \cdot (\rho_a c_a \vec{v} T_a) = \nabla \cdot (k_a \nabla T_a) \quad (4)$$

Momentum conservation equation:

$$\rho_a \frac{d\vec{v}}{dt} = -\nabla p + \mu_a \nabla^2 \vec{v} \quad (5)$$

or:

$$\rho_a \mu_j \frac{\partial \mu_i}{\partial \mu_j} = -\frac{\partial P}{\partial x_i} + \frac{\partial}{\partial x_j} \left[(\mu + \mu_j) \frac{\partial \mu_i}{\partial \mu_j} \right] \quad (6)$$

Turbulent kinetic energy equation:

$$\frac{\partial}{\partial t} (\rho k) + \frac{\partial}{\partial x_j} (\rho k \mu_j) = \frac{\partial}{\partial x_j} \left(\left(\mu + \frac{\mu_t}{\alpha_k} \right) \frac{\partial k}{\partial x_j} \right) + G_k + G_b - \rho \varepsilon - Y_M + S_k \quad (7)$$

Turbulent kinetic energy dissipation equation:

$$\frac{\partial}{\partial t} (\rho \varepsilon) + \frac{\partial}{\partial x_j} (\rho \varepsilon \mu_j) = \frac{\partial}{\partial x_j} \left(\left(\mu + \frac{\mu_t}{\alpha_\varepsilon} \right) \frac{\partial \varepsilon}{\partial x_j} \right) + C_{1\varepsilon} \frac{\varepsilon}{k} (G_k + C_{3\varepsilon} + G_b) - \rho C_{2\varepsilon} \frac{\varepsilon^2}{k} - S_\varepsilon \quad (8)$$

where ρ_a , C_a , k_a , and μ_a represent the mass density, specific heat, thermal conductivity, and dynamic viscosity of the cooling air, respectively; \vec{v} , T_a , and p represent the velocity, temperature, and static pressure, respectively; k and ε are, respectively, the turbulent kinetic energy and turbulent dissipation rate; μ_i and μ_j are the component of the velocity vector; μ and μ_t are the molecular and turbulent dynamic viscosity, respectively; G_k and G_b are, respectively, the turbulent kinetic energy generation result of mean velocity and the turbulent kinetic energy caused by buoyancy effects; Y_M is the contribution of fluctuating dilatation incompressible turbulent to the total dissipation rate; S_k and S_ε are, respectively, the source terms of k and ε ; α_k and α_ε represent the inverse effective Prandtl numbers, which are constant; $C_{1\varepsilon}$, $C_{2\varepsilon}$, and $C_{3\varepsilon}$ are the empirical parameters.

The above equations were solved by the SIMPLE algorithm in the CFD software ANSYS-FLUENT; furthermore, the central-differencing and second-order upwind schemes were employed to discretize the diffusive terms and convective terms. For the definition of the boundary, the velocity-inlet and pressure-outlet were selected, and the ambient pressure was set to atmosphere pressure. The surrounding wall was set to be adiabatic. Additionally, the following assumptions were considered in the simulation:

- (1) The physical properties of the air and batteries are constant;
- (2) the battery module is considered as a constant heat source and the heat generation rate is constant;
- (3) the ambient temperature and pressure are constant.

The simulation stops when the iteration residuals of continuity and energy equations fall below 10^{-4} and 10^{-6} , respectively.

2.2.2. Grid Independence Analysis

For the same air-cooled BTMS, Chen et al. [11] have verified that under the same conditions, there was a very small error of the CFD calculation results between the 2D model and 3D model, which was acceptable. Therefore, in this study, due to the fewer grids, the 2D calculation model of the air-cooled BTMS was adopted to save the calculation time. The grid and partial enlargement of the model are shown in Figure 3. The grid of the

boundary layer was encrypted. Parallel plates only serve a function of changing the flow pattern in this study. Under the premise of ensuring accuracy, to reduce the number of grids and enhance the calculation efficiency, a grid independence analysis study was done. The maximum temperature and minimum temperature of the battery pack were used to examine the grid independence. Figure 4 shows the variation of two values as the number of grids increases; it can be found that when the number of grids is larger than 73,272, the maximum temperature and minimum temperature of the battery pack change less than 0.02 and 0.03 K, respectively. Thus, a similar grid size was adopted in the following study.

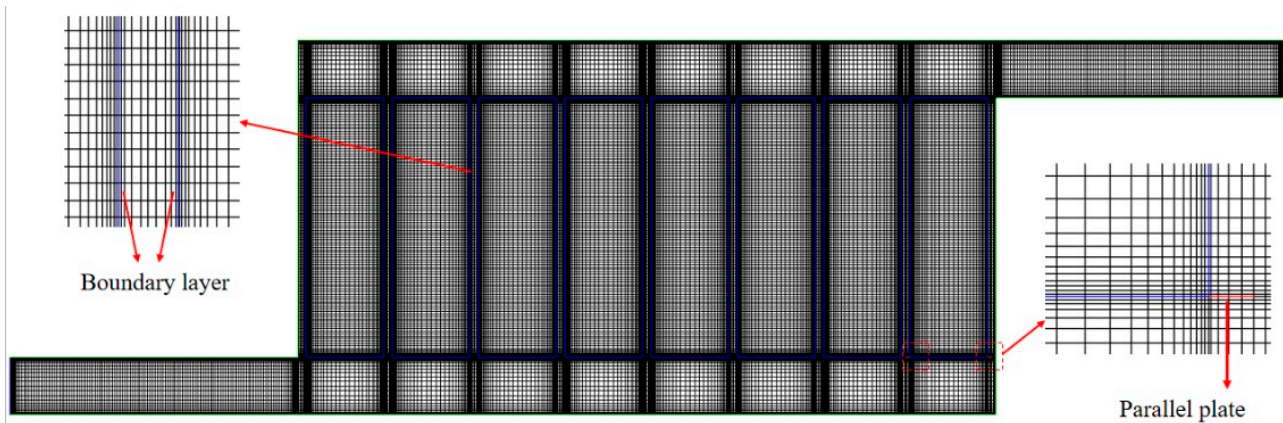


Figure 3. Grid and partial enlargement of the model.

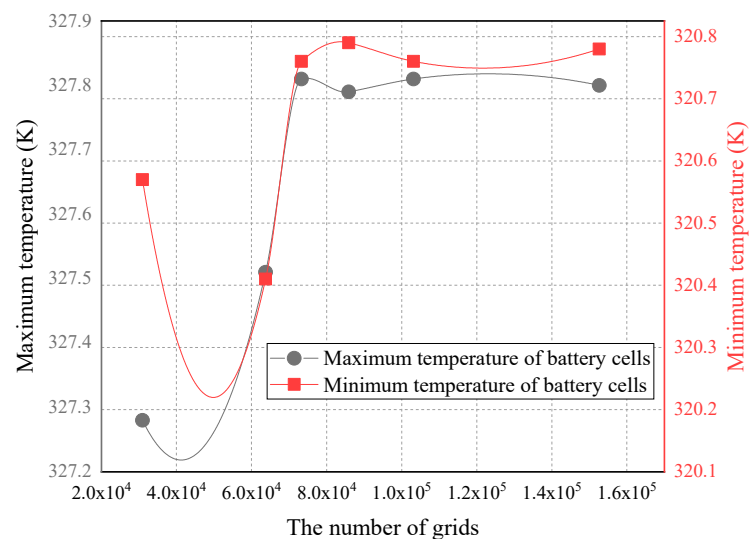


Figure 4. Simulation results of the basic model under different grid numbers.

2.2.3. Validation of the Computational Fluid Dynamics (CFD) Method

Chen et al. [11] replaced the batteries with aluminum blocks, and the same model of this study was investigated by experiment. Under the condition of inlet airflow velocity of 3, 3.5, and 4 m/s, the temperature of the center of each block's surface was measured. The details about the experiment can be found in [11]. To verify the feasibility of the CFD method in this paper, the simulation was carried out under the same experiment parameters. The maximum temperature and minimum temperature of the battery pack were chosen as the target parameters, and the results show that both for experiment and simulation, the highest and lowest temperature are located at the second and eighth battery cell, respectively. The comparison of the simulation results and experimental results are shown in Figure 5; as it can be seen, the error of the highest and lowest temperature is

within 0.47% and 0.26%, respectively, which is acceptable. Thus, the CFD method used in this paper is feasible.

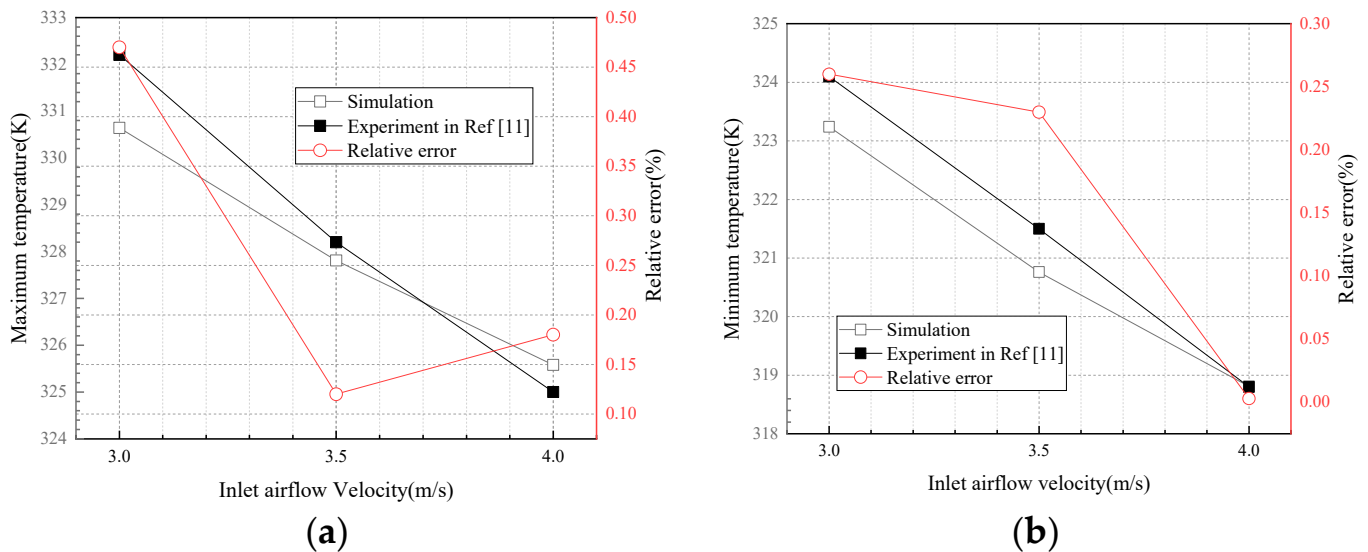


Figure 5. Comparison between the simulation results and experimental results; (a) maximum temperature and its relative error; (b) minimum temperature and its relative error.

3. Results and Discussions

3.1. Install Parallel Plate to the Cooling Channel from High Air Velocity to Low Air Velocity

The flow and temperature fields of the basic model are shown in Figure 6. It can be seen in Figure 6a that the airflow velocities in the cooling channel near the air inlet are low, while those away from the air inlet are high, which leads to the temperature of the battery cells near the air inlet being high and those away from the air inlet being low; the temperature contour is shown in Figure 6b. To ensure the temperature uniformity of the battery pack, the airflow velocity in each cooling channel should be uniform. According to the above analysis of the basic model, to reduce the airflow velocity of those cooling channels with high airflow velocity, the parallel plates were installed in the cooling channel with high airflow velocity, and the installation location was the battery side. Figure 2 shows the installation details; the length and height were initially set to 1.5 and 0 mm, respectively. The effect of the number of parallel plates on temperature performance was studied. Parallel plates were gradually added from the cooling channel with the highest airflow velocity to the lowest airflow velocity; the number of parallel plates gradually increased from 0 to 9, and the corresponding cases were denoted as case0 to case9. For example, when two parallel plates were installed, the first parallel plate was added in the highest airflow velocity cooling channel, and the second parallel plate was added in the second-highest airflow velocity cooling channel, and this case was denoted as case2, as can be seen in Figure 2. T_{\max} , ΔT_{\max} , and ΔP of the battery pack under various numbers of parallel plates are shown in Figure 7; as can be seen, the cooling efficiency of the BTMS can be significantly improved by installing parallel plates. T_{\max} and ΔT_{\max} of the battery pack were both reduced compared to the original model. As the number of parallel plates increased, T_{\max} and ΔT_{\max} first decreased, then increased and decreased finally, showing an s-shaped trend; ΔP increased gradually. Regardless of the pressure drop, case9 achieved the best battery performance; the smallest T_{\max} and ΔT_{\max} were both obtained, and the values were 325.06 and 3.01 K, respectively. However, the pressure drop of case9 was 34.76 Pa, which is 1.5 times more than the basic model. Considering the pressure drop within an acceptable range, case2 showed a better cooling performance with a lower ΔP increase, and the values of T_{\max} and ΔT_{\max} were 325.39 and 3.89 K, respectively, which were reduced by 2.42 and 3.76 K, respectively, compared to the basic model. Figure 8 shows

the flow and temperature fields of case2. As can be seen in Figure 8a, compared to the basic model shown in Figure 6a, a marked change in the velocity distribution can be found; the airflow velocity in the cooling channel where the parallel plates are located decreased significantly, which led to an obvious increase in the temperature of the battery cell at the corresponding position; the temperature distribution of case2 is shown in Figure 8b.

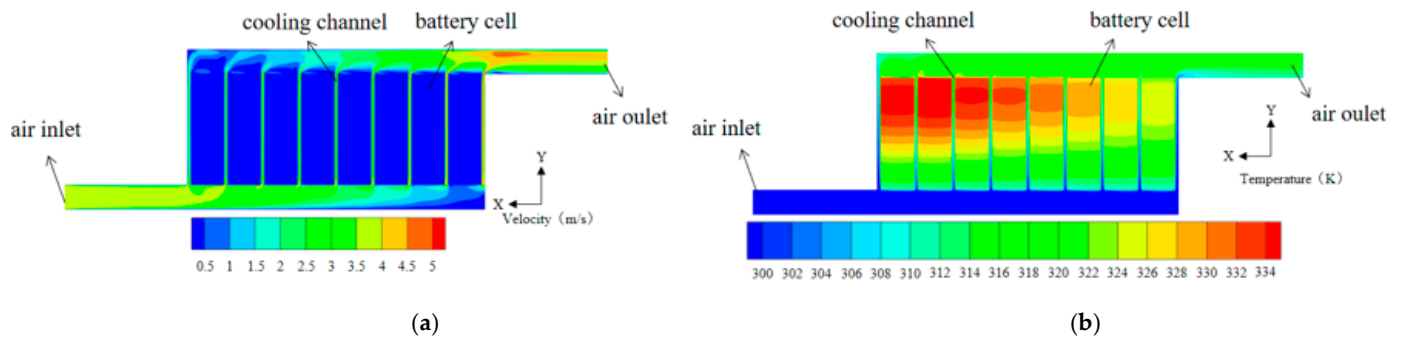


Figure 6. Flow and temperature fields of the basic model; (a) velocity contour of the basic model; (b) temperature contour of the basic model.

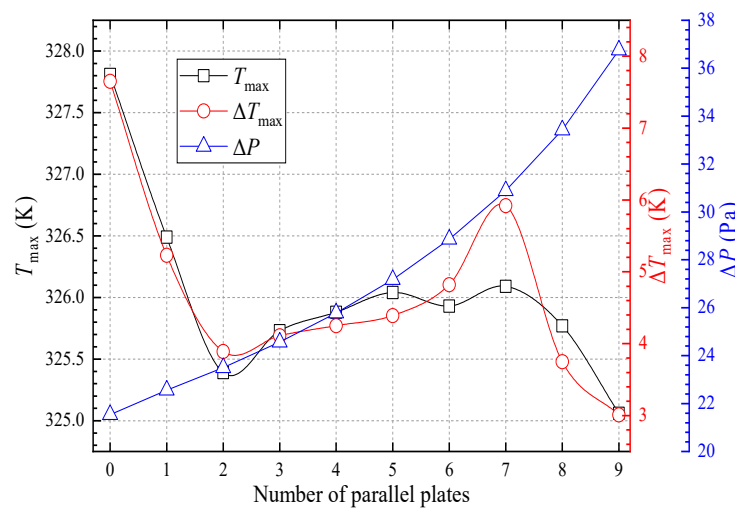


Figure 7. T_{max} , ΔT_{max} , and ΔP of the battery pack under various numbers of parallel plates.

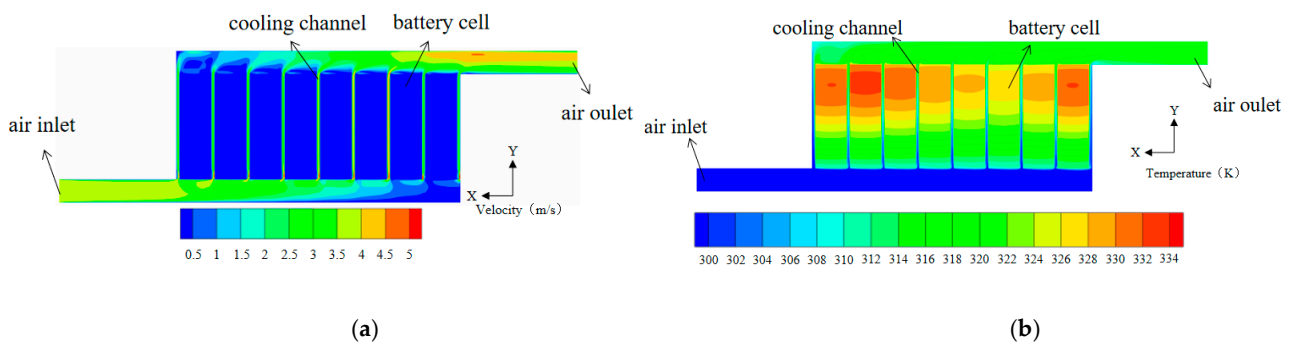


Figure 8. Flow and temperature fields of case2; (a) velocity contour of case2; (b) temperature contour of case2.

The temperature of each battery cell was associated with the airflow velocity on both sides of the battery cell; the greater the airflow velocity, the larger the Reynolds number and the larger the heat transfer coefficient, and a high cooling efficiency was achieved. The airflow distribution of case0, case2, case5, and case9 are depicted in Figure 9. As can be

seen, the airflow distribution was obviously changed after adding the parallel plates; the airflow velocities of those cooling channels with parallel plates were significantly reduced, while those without parallel plates were increased. As a result, the temperature uniformity of the system was improved. According to the s-shaped trend shown in Figure 7, when the number of parallel plates exceeded 2, the position of the highest temperature battery cell was changed. The reason can be summarized as follows: some battery cells have parallel plates installed on their sides, and the airflow velocities in those cooling channels with parallel plates drop too much so that the temperature of the current battery cell increases too much and exceeds the original highest temperature. ΔT_{\max} is also increased, until the number of parallel plates exceeds 7 and the turning point appears again; this is due to the disappearance of the above phenomena.

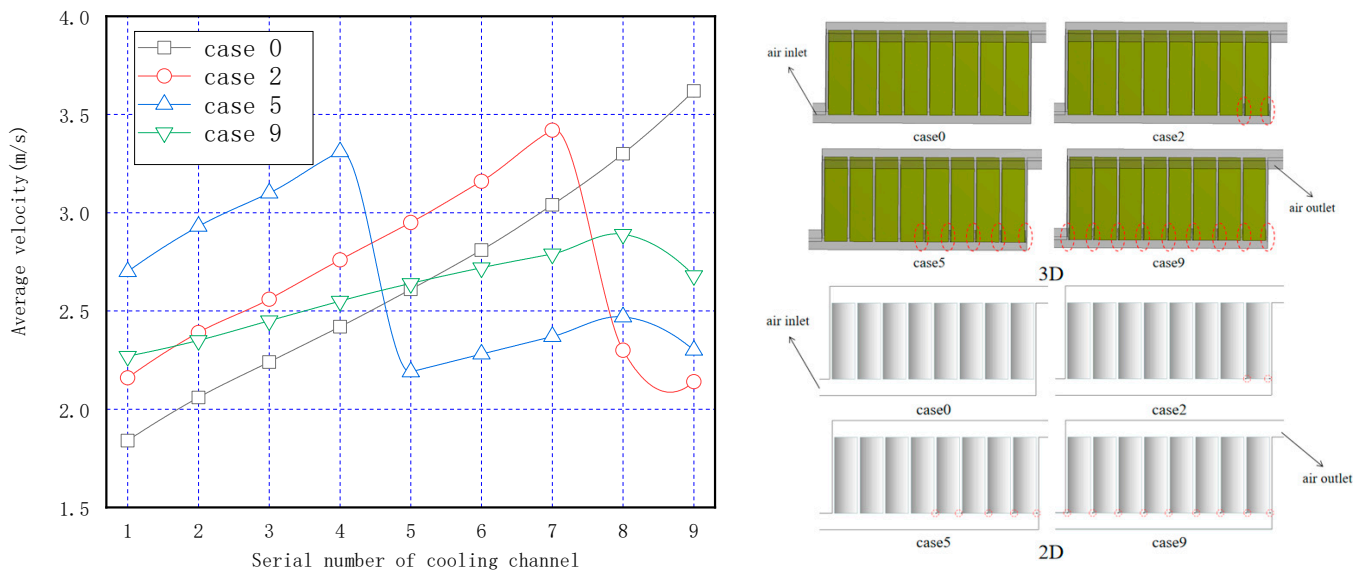
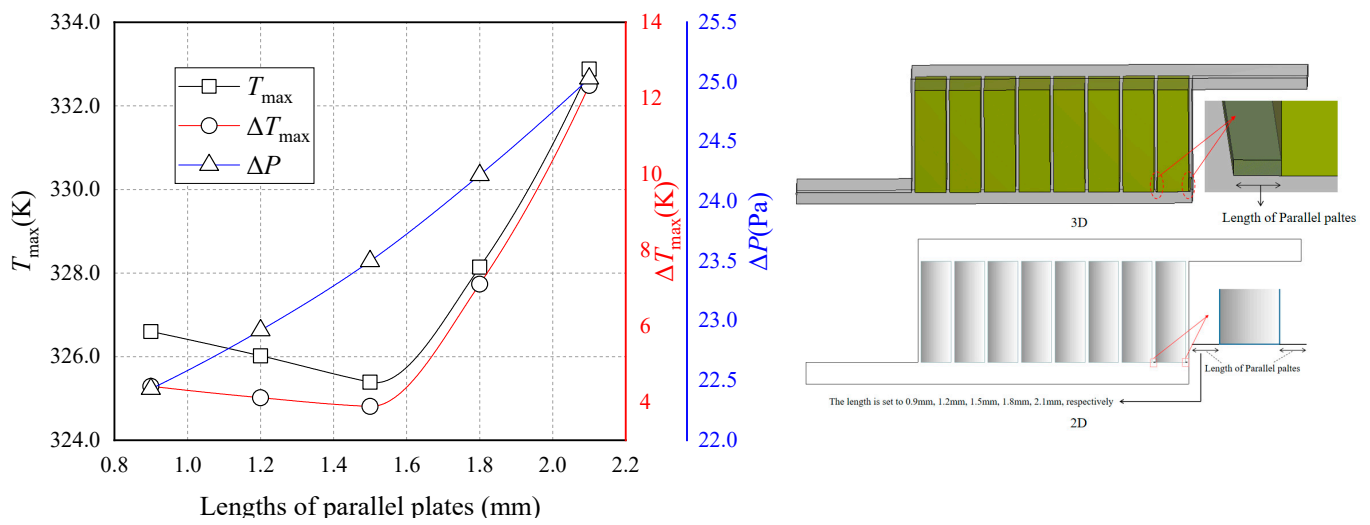


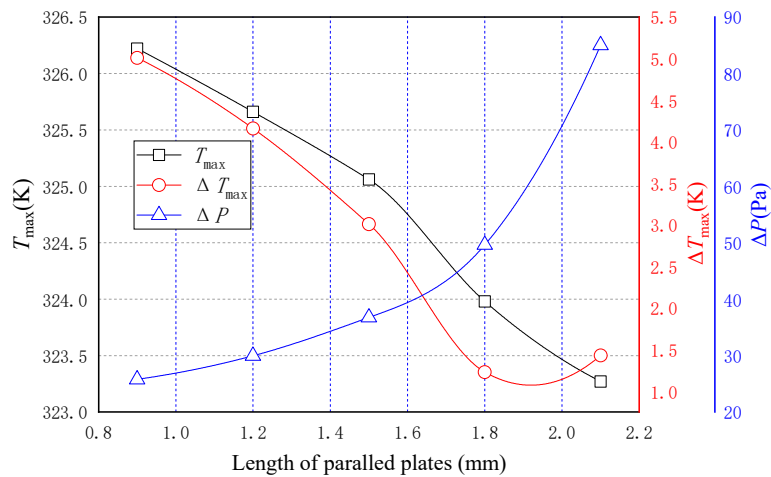
Figure 9. Airflow average velocities in nine channels for various cases.

3.2. The Influence of the Length of Parallel Plates

According to the above analysis, the models with two and nine parallel plates (case2 and case9) were chosen as objects of the following research; other conditions remained unchanged. The influence of the length of parallel plates on cooling performance was studied, and the calculation results are shown in Figure 10. The length of all parallel plates was changed at the same time from 0.9 to 2.1 mm with a 0.3 mm step size. As can be seen in Figure 10a, for the model with two parallel plates, when the length of parallel plates was 1.5 mm, the values of T_{\max} and ΔT_{\max} are both the lowest; they were 325.39 and 3.89 K, respectively. As can be seen in Figure 10b, for the model with nine parallel plates, when the length of parallel plates was 2.1 and 1.8 mm, respectively, the values of T_{\max} and ΔT_{\max} both reach the minimum; the values were 323.27 and 1.23 K, respectively. Both for case2 and case9, as the length of parallel plates increased, the pressure drop increased gradually; the reason is that the longer the parallel plates, the greater the resistance to airflow.



(a)



(b)

Figure 10. T_{max} , ΔT_{max} , and ΔP of the battery pack under various lengths of parallel plates; (a) cooling performance in case2 under various lengths of parallel plates; (b) cooling performance in case9 under various lengths of parallel plates.

Figure 11 shows the influence of the length of parallel plates on temperature and velocity distribution of the model. For case2, under various lengths of parallel plates, the temperatures of eight battery cells are depicted in Figure 11a, and the average velocity in each cooling channel is depicted in Figure 11b. As the length of parallel plates increased, the resistance to airflow became greater; the average velocity in the cooling channel with parallel plates installed was significantly reduced, which caused the temperature of the corresponding battery cell to rise; there was a slight increase in the average velocity in other cooling channels, so the temperature of other battery cells had a slight drop. The turning point was 1.5 mm for the five length parameters. It can be found that when the length of parallel plates was greater than 1.5 mm, the temperature of the eighth battery cell increased too much, exceeding the temperature of the second battery cell (the previous hottest battery cell) and becoming the highest temperature, and a higher temperature difference of the battery pack was also produced. For case9 (each cooling channel has installed a parallel plate), the calculation results are shown in Figure 11c,d. As the length of parallel plates increased, the velocity distribution of the battery pack became more uniform; meanwhile, T_{max} of the battery pack was gradually reduced; however, to obtain the good temperature performance, the power consumption caused by excessive pressure drop was unacceptable.

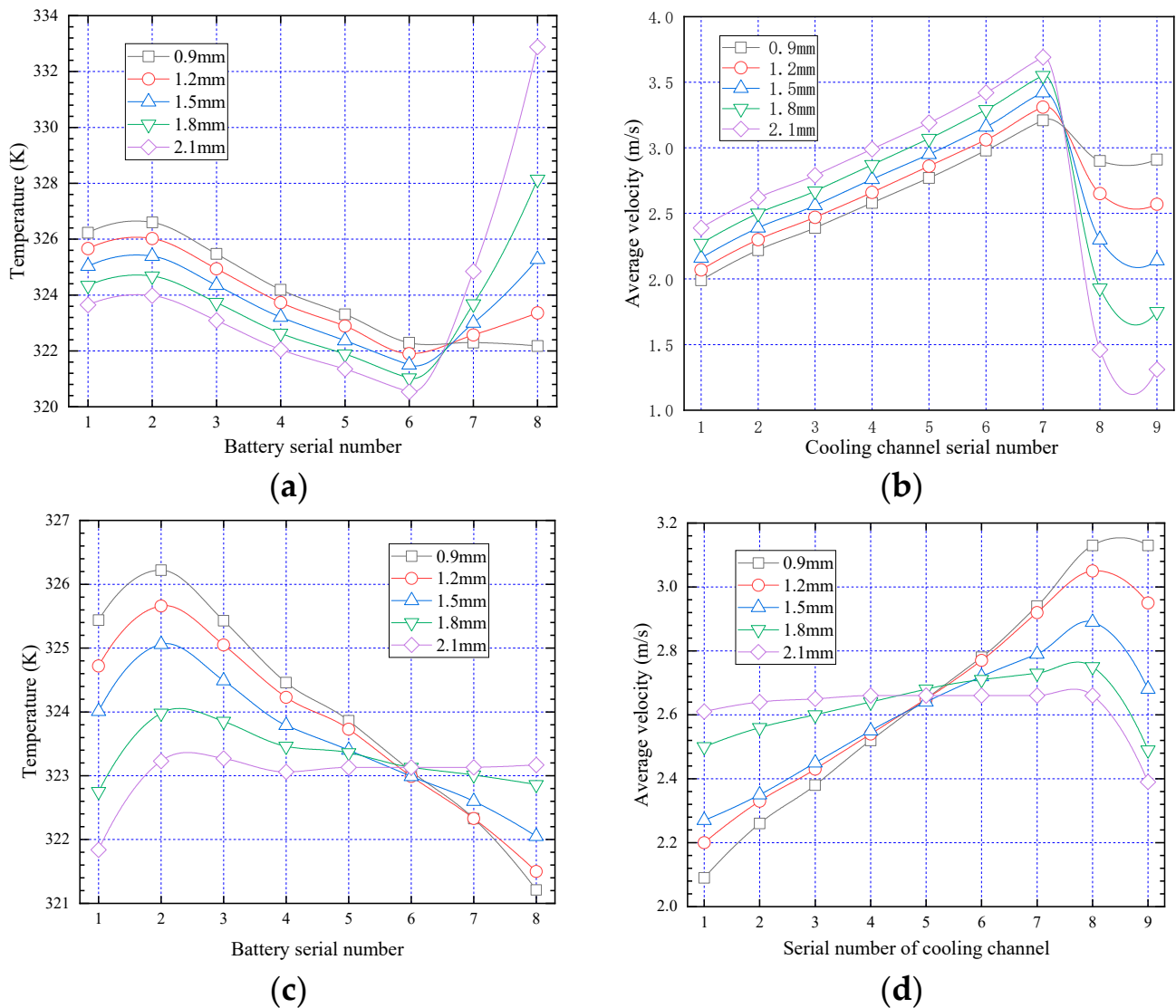
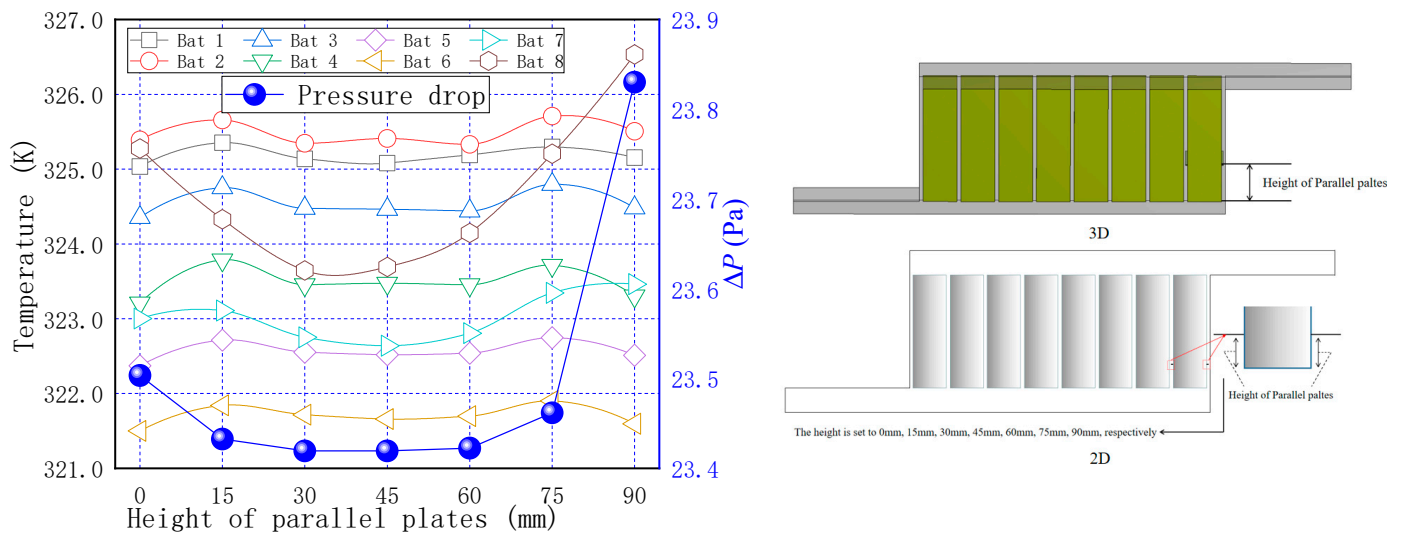


Figure 11. Effect of the length of parallel plates on temperature and velocity distribution of the model; (a) temperature distribution in case2; (b) velocity distribution in case2; (c) temperature distribution in case9; (d) average distribution in case9.

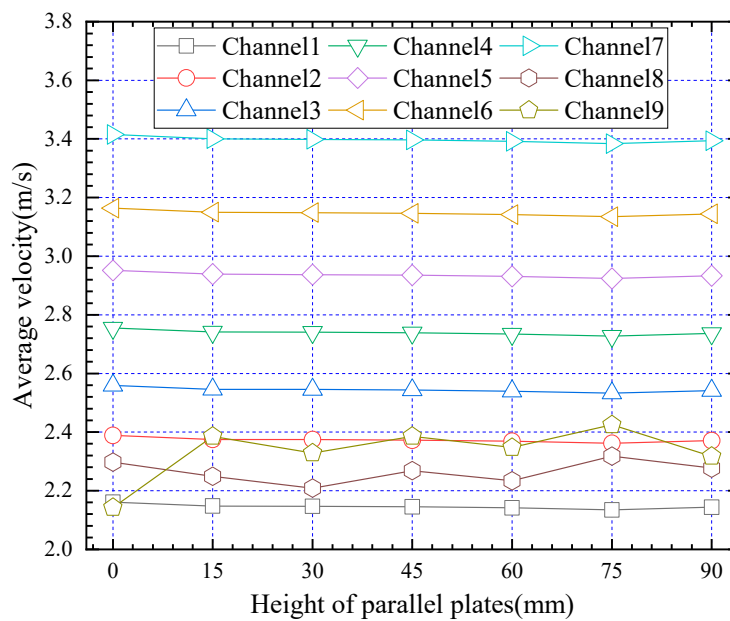
3.3. The Influence of the Position of Parallel Plates

Due to the best cooling performance, the BTMS with two 1.5 mm parallel plates (case2) was chosen as the next research object. The effect of the installation position of parallel plates was studied. In the above study, the parallel plate was installed at the bottom side of the battery. In this section, as shown in Figure 2, the height of parallel plates was changed at the same time from 0 to 90 mm with a 15 mm step size, and the calculation results about the temperature and velocity distribution of the battery pack are shown in Figure 12. As shown in Figure 12a, only the temperature of and seventh battery cell fluctuated considerably, the maximum fluctuation was 2.89 and 0.82 K, respectively, and the eighth battery temperature presented a lower value when the height was 30 or 45 mm. Other battery cells' temperature all kept the fluctuation within 0.5 K. The pressure drop was less affected by the installation height of parallel plates, it showed a trend of decreasing first and then rising. Figure 12b compares the airflow average velocity in each cooling channel with various installation heights of parallel plates; it can be found that the airflow average velocity in the cooling channel8 and cooling channel9 had an obvious fluctuation, while the airflow average velocity in other cooling channels was stable. As we know, parallel plates were added in the cooling channels on the sides of the eighth battery cell, so the conclusion was drawn

as follows: the temperature of those battery cells with added parallel plates on the side is significantly influenced by the installation height of parallel plates.



(a)



(b)

Figure 12. Effect of parallel plates installation height on cooling performance of the model; (a) cooling performance of the model under various installation height of parallel plates; (b) airflow distribution of the model under various installation height of parallel plates.

3.4. Optimization Based on the Model with Four Parallel Plates

To verify the applicability of the conclusions obtained above, case4 was chosen as the research object, and three optimization schemes were put forward according to the above conclusions, which were, respectively, denoted as case4-opt1, case4-opt2, and case4-opt3; the specific measures corresponding to each scheme are depicted in Table 1, and the values of T_{max} , ΔT_{max} , and ΔP of the battery pack in each case are also summarized. Figure 13 shows the calculation results about the temperature of the eight battery cells. As can be seen in Figure 13, the temperature distribution of the module was changed

significantly after optimization; T_{\max} and ΔT_{\max} of the battery pack were smaller than those before optimization. It can also be found that the temperature of all battery cells in case4-opt2 was lower than those in case4. In Table 1, the pressure drop of three optimization systems fluctuated by a range of about 1.5 Pa compared to case4; therefore, the influence of the power consumption was small and negligible. The values of T_{\max} and ΔT_{\max} of the case4-opt3 both were the smallest; they were 324.44 and 2.15 K, respectively, which were reduced by 1.44 and 2.16 K, respectively. Figure 14 shows the temperature contours of four cases, which clearly describes the temperature changes of case4 under three optimization schemes; the temperature of the sixth and seventh battery cells dropped significantly, and the temperature distribution became more uniform.

Table 1. Specific measures corresponding to each scheme.

Case	Height of Parallel Plates	Length of Parallel Plates	Tmax (K)	ΔT_{\max} (K)	ΔP (Pa)
Case4	Set all to 0 mm	Set all to 1.5 mm	325.88	4.31	25.78
Case4-opt1	Set all to 0 mm	Set all to 1.2 mm	324.73	2.20	24.35
Case4-opt2	Set the first three (from left to right) to 30 mm, set the fourth to 0 mm.	Set all to 1.5 mm	324.59	3.05	26.07
Case4-opt3	Set the first three (from left to right) to 30mm, set the fourth to 0 mm.	Set all to 1.2 mm	324.44	2.15	24.29

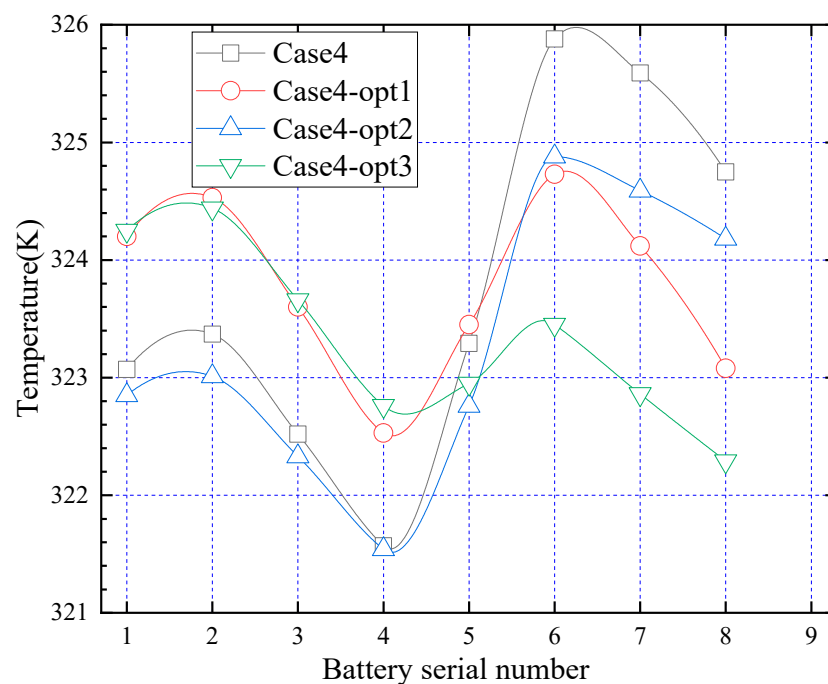


Figure 13. Temperature of eight battery cells in each case.

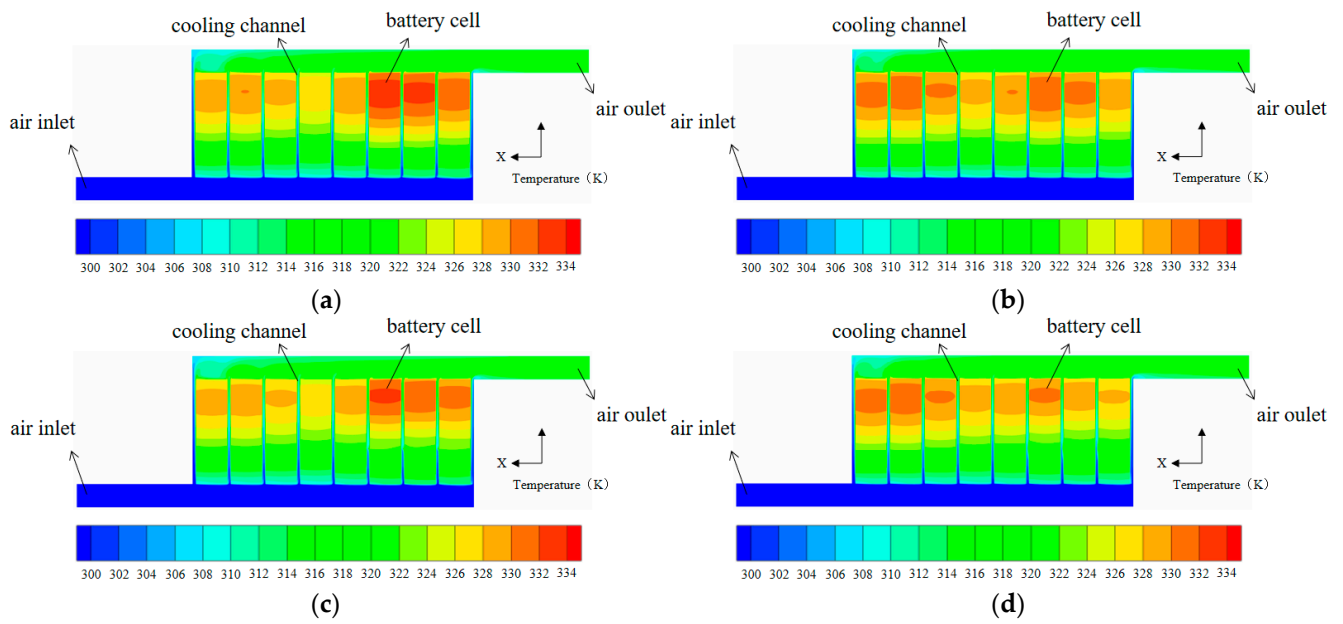


Figure 14. Temperature contours of four cases; (a) case4; (b) case4-opt1; (c) case4-opt2; (d) case4-opt3.

For those optimal and basic systems, the calculation results about T_{max} and ΔT_{max} of the battery pack under various inlet airflow velocities are shown in Figure 15. As can be seen in Figure 15, as the inlet airflow velocity increased, T_{max} of all cases had a certain degree of reduction, but ΔT_{max} was not sensitive and stayed relatively stable. The best cooling efficiency was obtained by case4-opt3 at different inlet airflow velocities. Hence, the above conclusions can be applied to other situations effectively.

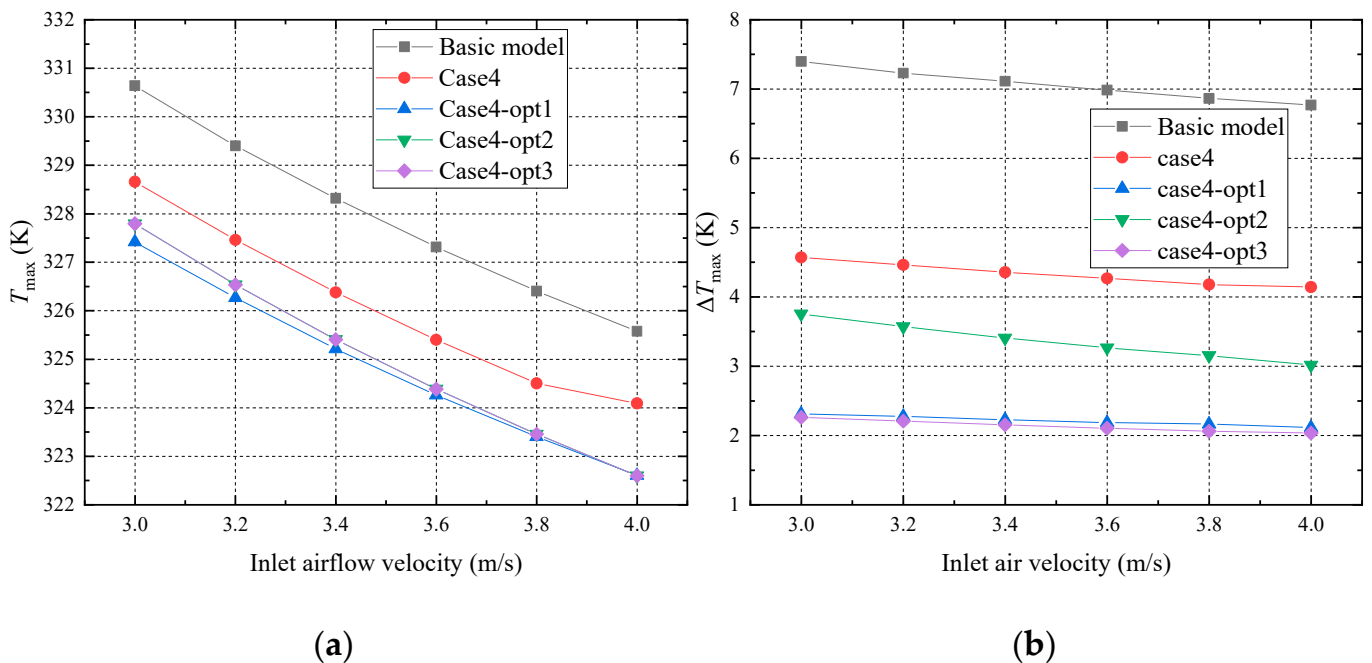


Figure 15. Comparison of T_{max} and ΔT_{max} in different cases under various inlet airflow velocities; (a) T_{max} of various cases; (b) ΔT_{max} of various cases.

4. Conclusions

In this paper, parallel plates were introduced to change the airflow distribution of the battery pack, and the cooling efficiency was effectively improved. The CFD method was verified by the experiment results, so the flow and temperature fields were obtained by simulation. Firstly, the effect of the number of parallel plates on cooling performance was studied. The best cooling performance case was always selected as the next research object. Secondly, the effects of the length and height of parallel plates on cooling efficiency were investigated. Finally, three optimization schemes were designed for one previous case (case4), and the validity of the conclusions was verified. The following findings and conclusions can be obtained in this study.

- (1) The cooling performance of the BTMS can be significantly improved by adding the parallel plates. The effect of the number of parallel plates on cooling performance was investigated; when the number of parallel plates was nine, T_{\max} and ΔT_{\max} were both lowest, but ΔP increased greatly. Considering the acceptable range of power consumption loss, the best cooling efficiency was obtained by the model with two parallel plates; T_{\max} and ΔT_{\max} of the battery pack were, respectively, reduced by 2.42 and 3.46 K compared to the original model.
- (2) As the length of parallel plates increased, the pressure drop gradually increased. For the model with two parallel plates, the best cooling performance was obtained when the length of parallel plates was 1.5 mm. For the model with nine parallel plates, to obtain the good temperature performance, the power consumption caused by excessive pressure drop was unacceptable.
- (3) With the increase of the height of parallel plates, the temperature of the battery cell without adding parallel plates was insensitive; instead, the temperature of the battery cell with parallel plates added on the side fluctuated significantly, showing a trend of decreasing first and then rising.
- (4) The cooling performance of the battery pack can be improved by the optimization schemes designed in this paper. For those cases, T_{\max} and ΔT_{\max} of the battery pack of the third optimization system were, respectively, reduced by 3.37 and 5.5 K compared to the original model, which achieved the best cooling performance. The temperature uniformity of all cases remained stable for the various inlet airflow velocities.

Author Contributions: Conceptualization, M.W. and H.X.; methodology, M.W., T.-C.H. and H.X.; software, M.W.; validation, M.W. and H.X.; formal analysis, T.-C.H. and H.X.; investigation, M.W.; resources, H.X.; data curation, M.W.; writing—original draft preparation, M.W.; writing—review and editing, M.W. and H.X.; visualization, H.X.; supervision, H.X.; project administration, H.X.; finding acquisition, H.X. All authors have read and agreed to the published version of the manuscript.

Funding: This work was supported by the National Natural Science Foundation of China (Nos. 52076163, 51706176), the Key Research and Development Program of Shaanxi (No. 2020SF-404), and the National Postdoctoral Program for Innovative Talents (No. BX20200265).

Institutional Review Board Statement: Not applicable.

Informed Consent Statement: Not applicable.

Data Availability Statement: Not applicable.

Acknowledgments: This work was supported by the National Natural Science Foundation of China (Nos. 52076163, 51706176), the Key Research and Development Program of Shaanxi (No. 2020SF-404), and the National Postdoctoral Program for Innovative Talents (No. BX20200265). The support is gratefully acknowledged.

Conflicts of Interest: The authors declare no conflict of interest.

References

1. Greco, A.; Jiang, X.A. Coupled thermal and electrochemical study of lithium-ion battery cooled by paraffin/porous-graphite-matrix composite. *J. Power Sources* **2016**, *315*, 127–139. [[CrossRef](#)]
2. Na, X.; Kang, H.; Wang, T.; Wang, Y. Reverse layered air flow for Li-ion battery thermal management. *Appl. Therm. Eng.* **2018**, *143*, 257–262. [[CrossRef](#)]
3. Dan, D.; Yao, C.; Zhang, Y.; Zeng, Z.; Xu, X. Dynamic thermal behavior of micro heat pipe array-air cooling battery thermal management system based on thermal network model. *Appl. Therm. Eng.* **2019**, *162*, 114183. [[CrossRef](#)]
4. Mahamud, R.; Park, C. Reciprocating air flow for Li-ion battery thermal management to improve temperature uniformity. *J. Power Sources* **2011**, *196*, 5685–5696. [[CrossRef](#)]
5. Liu, Y.; Zhang, J. Design a J-type air-based battery thermal management system through surrogate-based optimization. *Appl. Energy* **2019**, *252*, 113426. [[CrossRef](#)]
6. Behi, H.; Karimi, D.; Behi, M.; Ghanbarpour, M.; Jaguemont, J.; Sokkeh, M.A.; Gandoman, F.H.; Berecibar, M.; Van Mierlo, J. A new concept of thermal management system in Li-ion battery using air cooling and heat pipe for electric vehicles. *Appl. Therm. Eng.* **2020**, *174*, 115280. [[CrossRef](#)]
7. Pesaran, A.A. Battery thermal models for hybrid vehicle simulations. *J. Power Sources* **2002**, *110*, 377–382. [[CrossRef](#)]
8. Severino, B.; Gana, F.; Palma-Behnke, R.; Estévez, P.A.; Calderón-Muñoz, W.R.; Orchard, M.E.; Reyes, J.; Cortés, M. Multi-objective optimal design of lithium-ion battery packs based on evolutionary algorithms. *J. Power Sources* **2014**, *267*, 288–299. [[CrossRef](#)]
9. Chen, K.; Wang, S.; Song, M.; Chen, L. Configuration optimization of battery pack in parallel air-cooled battery thermal management system using an optimization strategy. *Appl. Therm. Eng.* **2017**, *123*, 177–186. [[CrossRef](#)]
10. Wang, T.; Tseng, K.; Zhao, J.; Wei, Z. Thermal investigation of lithium-ion battery module with different cell arrangement structures and forced air-cooling strategies. *Appl. Energy* **2014**, *134*, 229–238. [[CrossRef](#)]
11. Chen, K.; Wu, W.; Yuan, F.; Chen, L.; Wang, S. Cooling efficiency improvement of air-cooled battery thermal management system through designing the flow pattern. *Energy* **2019**, *167*, 781–790. [[CrossRef](#)]
12. Hong, S.; Zhang, X.; Chen, K.; Wang, S. Design of flow configuration for parallel air-cooled battery thermal management system with secondary vent. *Int. J. Heat Mass Transf.* **2018**, *116*, 1204–1212. [[CrossRef](#)]
13. Shahid, S.; Agelin-Chaab, M. Development and analysis of a technique to improve air-cooling and temperature uniformity in a battery pack for cylindrical batteries. *Therm. Sci. Eng. Prog.* **2018**, *5*, 351–363. [[CrossRef](#)]
14. Park, H. A design of air flow configuration for cooling lithium ion battery in hybrid electric vehicles. *J. Power Sources* **2013**, *239*, 30–36. [[CrossRef](#)]
15. Xie, J.; Ge, Z.; Zang, M.; Wang, S. Structural optimization of lithium-ion battery pack with forced air cooling system. *Appl. Therm. Eng.* **2017**, *126*, 583–593. [[CrossRef](#)]
16. Chen, K.; Li, Z.; Chen, Y.; Long, S.; Hou, J.; Song, M.; Wang, S. Design of Parallel Air-Cooled Battery Thermal Management System through Numerical Study. *Energies* **2017**, *10*, 1677. [[CrossRef](#)]
17. Shahid, S.; Agelin-Chaab, M. Experimental and numerical studies on air cooling and temperature uniformity in a battery pack. *Int. J. Energy Res.* **2018**, *42*, 2246–2262. [[CrossRef](#)]
18. Zhang, F.; Lin, A.; Wang, P.; Liu, P. Optimization design of a parallel air-cooled battery thermal management system with spoilers. *Appl. Therm. Eng.* **2021**, *182*, 116062. [[CrossRef](#)]
19. Li, W.; Xiao, M.; Peng, X.; Garg, A.; Gao, L. A surrogate thermal modeling and parametric optimization of battery pack with air cooling for EVs. *Appl. Therm. Eng.* **2019**, *147*, 90–100. [[CrossRef](#)]